IEEE Access
Multidisciplinary | Rapid Review | Open Access Journal

Received November 8, 2019, accepted November 23, 2019, date of publication December 4, 2019,
date of current version December 31, 2019.

Digital Object Identifier 10.1109/ACCESS.2019.2957122

Analysis and Design of Wideband 90° Microstrip Hybrid Coupler

RUYING SUN[1,2], QINGHU CHEN[1], RONGCANG HAN[2], AND ZHONGLIANG LU[3]
[1]School of Electronic Information, Wuhan University, Wuhan 430072, China
[2]School of Physics and Electronic Engineering, Linyi University, Linyi 276005, China
[3]School of Information Engineering, Jiangxi University of Science and Technology, Ganzhou 341000, China

Corresponding authors: Qinghu Chen (qhchen@whu.edu.cn) and Rongcang Han (hg198172@163.com)

This work was supported by the National Natural Science Foundation of China under Grant 61701203, and in part by the Research Start-Up Funding of Linyi University under Grant LYDX2017BS001.

ABSTRACT A wideband 90° microstrip hybrid coupler with a bandwidth of 84.3% is proposed. The hybrid coupler consists of a two-section coupled-line power divider and a 90° phase shifter. The two-section coupled-line is of natural broadband characteristics, and not only performs the role of impedance matching, but also makes the total circuit compact. The phase shifter employs a pair of open- and short-circuit stubs inserted into the reference transmission line to compensate the phase variation in proportion to the operating frequency for the conventional transmission line. Thus, the phase shifter possesses wideband performance on impedance matching as well as phase shifting. To prove the design methodology, a wideband 90° hybrid coupler operating at 3 GHz is designed and fabricated. In the case of −15 dB reflection coefficient for all ports of the coupler, the output maximum amplitude unbalance is less than 1 dB, the phase variation is less than 5 degree, and the port isolation is better than 18 dB.

INDEX TERMS Wideband hybrid coupler, broadband phase shifter, even- and odd-mode analysis.

I. INTRODUCTION

Hybrid couplers with 180° or 90° phase difference play an important role in microwave circuits. The hybrid coupler is a key component in balanced power amplifiers, modulators balanced mixers, and various antennas' feeding networks [1]–[5]. Specially, the 90° hybrid coupler with equal power division is often used in circularly polarized (CP) antenna systems [6]–[8], which can be realized in four-port or three-port structures. The branch-line directional coupler as a four-port 90° hybrid and the conventional design [9] is confined by a ∼20% impedance matching bandwidth and a ∼10% phase shifting bandwidth, only suitable for a narrow-band application. To meet the requirements of wideband systems, various techniques have been proposed to achieve wideband branch-line directional couplers [10]–[14]. The coupler with defected ground structure in [10] accomplishes a bandwidth of 43.3%, but the defected ground may lead to undesirable radiation problem. The branch-line coupler employs cascading multiple-section structure [11]–[12] achieved a fractional bandwidth of ∼56%, but suffers a severe restriction in fabrication. These results from the requirement that the microstrip line should be of very high impedance, i.e. extremely low aspect ratio or very thin conductor width. The multi-layer structure can greatly broaden the bandwidth [13]–[15], but multi-layer structure may increase circuit complexity and cause incompatibility with other components during circuit integration. The Lange coupler [16]–[19], which has been fabricated in a small size on the single layer PCB, has been suggested. Although it has wide band characteristics in a small size, it still has drawbacks that narrow line widths, narrow gaps between coupled lines for the tight coupling, and low power capability depending on substrates, and multiple wire-bonding are required.

Apart from the branch-line couplers, the hybrid coupler can also be accomplished in the three-port structure. This three-port structure consists of a balanced power divider and a phase shifter, and various hybrid couplers can be achieved by properly incorporating different phase shifters. For example, some wideband planar baluns have been implemented by adopting a Wilkinson power divider and a broadband 180° phase shifter [20], [21]. However, the efficient bandwidths are limited to ∼50% while port reflection coefficient less than −15 dB, which suffers from the bandwidth limita-

The associate editor coordinating the review of this manuscript and approving it for publication was Kuang Zhang.

This work is licensed under a Creative Commons Attribution 4.0 License. For more information, see http://creativecommons.org/licenses/by/4.0/

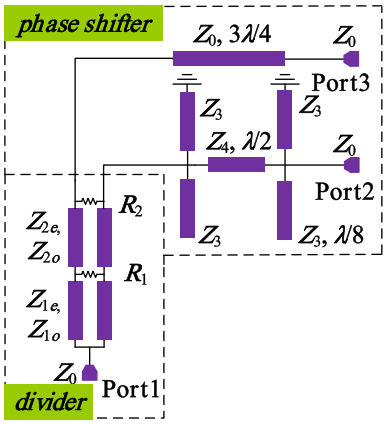

FIGURE 1. The equivalent circuit of the proposed Hybrid Coupler.

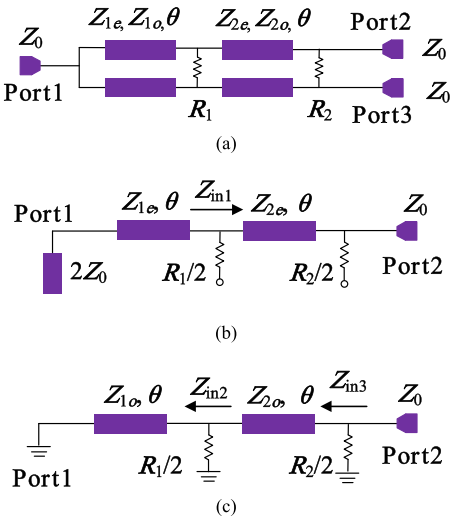

FIGURE 2. Configuration of the power divider (a) and its equivalent circuit in even- (b) and odd-mode (c) excitations.

tion of 50% ∼ 60% (reflection coefficient ≤−15 dB) for Wilkinson power divider [9]. The wideband coupler [22] realized by the coupled-line power divider which operating bandwidth is less than 50% because of the limitation of its phase shifting. Therefore, accomplishing a three-port wideband 90° hybrid coupler can be regarded as designing two key components, a broadband power divider and a broadband 90° phase shifter. Comparing with the design of a wideband power divider, achieving a broadband phase shifter is more technically challenging. So, various methods have been presented to improve the phase shifter performances [23]–[28]. For instance, the tight coupled-lines are employed in the Schiffman phase shifter [23], [24] to broaden the operating bandwidth, but the major drawback of which is difficult to be fabricated, while the modified Schiffman phase shifters with a defected ground structure in [25], [26] which may lead to serious radiation problems. Additionally, a lumped capacitor is utilized to broaden operating band in an improved Schiffman phase shifter [27]. However, in this case, the hybrid coupler is limited to relatively low frequency applications. Aperture coupling in multilayer structures is proved feasible to design ultra-wideband phase shifters [28], but it is incompatible with widely used single-layer components.

In this paper, a wideband 90° hybrid coupler composed of a broadband power divider and a broadband 90° phase shifter is proposed, whose equivalent circuit is illustrated in Fig. 1. This paper is organized as follows. Firstly, the detailed theoretical analysis and design procedure, including the odd- and even-mode analysis for the power divider and the phase shifter, are presented in Section II, respectively. Then, the simulated and measured results of the designed wideband 90° hybrid coupler are illustrated and discussed in Section III. At last, the summary of the paper is given in Section IV.

II. THEORETICAL ANALYSIS

A. THEORETICAL ANALYSIS OF POWER DIVIDER

This is a two-way symmetric power divider using a two-section coupled-line and two isolation resistors. Since all the transmission lines are coupled, the physical space between the two arms of the divider will be very close. Thus, the placement of two small-size lumped resistors is convenient without a ring structure for separating the two arms and mounting the resistors. This feature enables the operation at higher frequencies. These coupled-lines with characteristic impedances Z_{ie}, Z_{io} and electrical length θ, where $i = 1, 2$, perform the role of impedance matching. Moreover, two lumped resistors play a critical role in enhancing the isolation and output-port matching performances for this divider.

According to even- and odd-mode analysis, the circuit can be simplified to Fig. 2 (b) and (c) where the even- and odd-mode characteristic impedances of coupled lines are effectively separated for simplicity.

For a power divider with matched ports, the ideal input matching (Port 1 in Fig.2 (a)) is necessary. Hence, the following relationship of the parameters in Fig.2 (b) must be satisfied:

$$2Z_0 = Z_{1e}\frac{Z_{in1} + jZ_{1e}\tan\theta}{Z_{1e} + jZ_{in1}\tan\theta} \tag{1}$$

$$Z_{in1} = Z_{2e}\frac{Z_0 + jZ_{2e}\tan\theta}{Z_{2e} + jZ_0\tan\theta} \tag{2}$$

After substituting (2) into (1), separating the real and imaginary parts of the combined equation, assuming Z_0 and θ are known coefficients, Z_{1e} and Z_{2e} can be solved simultaneously.

$$\begin{cases} Z_{1e} = Z_0\sqrt{\dfrac{\sqrt{1+8\tan^4\theta}-1}{\tan^2\theta}} \\ Z_{2e} = Z_0\sqrt{\dfrac{\sqrt{1+8\tan^4\theta}+1}{2\tan^2\theta}} \end{cases} \tag{3}$$

Similarly, to satisfy the ideal matching and isolation performance between port 2 and port 3, namely, the reflection coefficient equals zero, the relationship of the mentioned

impedance parameters in Fig.2 (c) can be derived as

$$Z_{in2} = \frac{jR_1 Z_{1o}\tan\theta}{R_1 + j2Z_{1o}\tan\theta} \tag{4}$$

$$Z_{in3} = Z_{2o}\frac{Z_{in2} + jZ_{2o}\tan\theta}{Z_{2o} + jZ_{in2}\tan\theta} \tag{5}$$

$$Z_0 = \frac{R_2 Z_{in3}}{R_2 + 2Z_{in3}} \tag{6}$$

Next, the solutions for R_1 and R_2 are obtained from the odd mode requirements (4)–(6). They are given by the following set of equations.

$$\begin{cases} R_1 = \dfrac{2Z_{1o}Z_{2o}\tan^2\theta}{\sqrt{(Z_{1o}+Z_{2o})\tan^2\theta[Z_{1o}\tan^2\theta - Z_{2o}]}} \\ R_2 = \dfrac{2Z_0(Z_{1o}+Z_{2o})Z_{2o}^2\tan^2\theta}{(Z_{1o}Z_{2o}^2 - Z_0^2Z_{1o} + Z_{2o}^3)\tan^2\theta + Z_0^2Z_{2o}} \\ \quad + \dfrac{2Z_0^2Z_{2o}\sqrt{(Z_{1o}+Z_{2o})\tan^2\theta[Z_{1o}\tan^2\theta - Z_{2o}]}}{(Z_{1o}Z_{2o}^2 - Z_0^2Z_{1o} + Z_{2o}^3)\tan^2\theta + Z_0^2Z_{2o}} \end{cases} \tag{7}$$

$$S_{11e} = \frac{\begin{bmatrix} Z_0(2Z_{2e}^2 - Z_{1e}^2)\sin^2\theta - Z_0Z_{1e}Z_{2e}\cos^2\theta \\ +j(Z_{1e}+Z_{2e})(Z_{1e}Z_{2e} - 2Z_0^2)\sin\theta\cos\theta \end{bmatrix}}{\begin{bmatrix} 3Z_0Z_{1e}Z_{2e}\cos^2(\theta) - Z_0(Z_{1e}^2 + 2Z_{2e}^2)\sin^2\theta \\ +j(Z_{1e}+Z_{2e})(Z_{1e}Z_{2e} + 2Z_0^2)\sin\theta\cos\theta \end{bmatrix}} \tag{8}$$

$$S_{12e} = \frac{2\sqrt{2}\,Z_{1e}Z_{2e}Z_0}{\begin{bmatrix} 3Z_0Z_{1e}Z_{2e}\cos^2\theta - Z_0(Z_{1e}^2 + 2Z_{2e}^2)\sin^2\theta \\ +j(Z_{1e}+Z_{2e})(Z_{1e}Z_{2e} + 2Z_0^2)\sin\theta\cos\theta \end{bmatrix}} \tag{9}$$

$$S_{22e} = \frac{\begin{bmatrix} Z_0Z_{1e}Z_{2e}\cos^2\theta + Z_0(Z_{1e}^2 - 2Z_{2e}^2)\sin^2\theta \\ +j(Z_{1e}+Z_{2e})(Z_{1e}Z_{2e} - 2Z_0^2)\sin\theta\cos\theta \end{bmatrix}}{\begin{bmatrix} 3Z_0Z_{1e}Z_{2e}\cos^2\theta - Z_0(Z_{1e}^2 + 2Z_{2e}^2)\sin^2\theta \\ +j(Z_{1e}+Z_{2e})(Z_{1e}Z_{2e} + 2Z_0^2)\sin\theta\cos\theta \end{bmatrix}} \tag{10}$$

$$S_{22o} = \frac{\begin{bmatrix} (R_1R_2Z_0Z_{1o} - 2R_2Z_{1o}Z_{2o}^2 + 4Z_0Z_{1o}Z_{2o}^2)\sin^2\theta \\ -Z_0Z_{2o}R_1R_2\cos^2\theta + j(R_1R_2 - 2R_1Z_0)Z_{2o}^2\sin\theta\cos\theta \\ +jZ_{1o}Z_{2o}(R_1R_2 - 2R_1Z_0 - 2R_2Z_0)\sin\theta\cos\theta \end{bmatrix}}{\begin{bmatrix} -(R_1R_2Z_0Z_{1o} + 2R_2Z_{1o}Z_{2o}^2 + 4Z_0Z_{1o}Z_{2o}^2)\sin^2\theta \\ +Z_0Z_{2o}R_1R_2\cos^2\theta + j(R_1R_2 + 2R_1Z_0)Z_{2o}^2\sin\theta\cos\theta \\ +jZ_{1o}Z_{2o}(2R_1R_2 + 2R_1Z_2 + 2R_2Z_0)\sin\theta\cos\theta \end{bmatrix}} \tag{11}$$

Due to the symmetry of the circuit shown in Fig.2 (a), the following relationships can be derived: $S_{12} = S_{21} = S_{13} = S_{31}$, $S_{22} = S_{33}$, $S_{23} = S_{32}$. First, consider Fig. 2 (b), according to the transformation between scattering parameters and ABCD-matrix parameters [29], the closed form even-mode parameters can be simplified and summarized as (8)–(10). It is interesting that we can also obtain the odd-mode parameters S_{22o} (11) using the above similar manipulation when Fig.2 (c) is considered.

Therefore, the scattering parameters can be calculated by (12)–(15).

$$S_{11} = S_{11e} \tag{12}$$

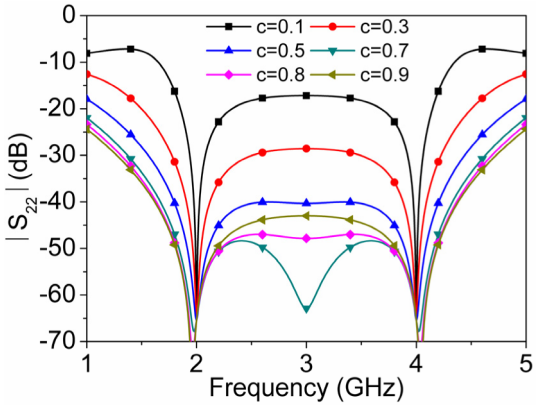

FIGURE 3. The relationship between Z_{io} ($i = 1.2$) and $|S_{22}|$ with $f_2/f_1 = 2$.

$$S_{12} = \frac{S_{12e}}{\sqrt{2}} \tag{13}$$

$$S_{22} = \frac{S_{22e} + S_{22o}}{2} \tag{14}$$

$$S_{23} = \frac{S_{22e} - S_{22o}}{2} \tag{15}$$

A careful examination of the solutions in (3) and (7) reveals that they are all even functions in $\tan\theta$. Therefore, the solutions do not change for two different values of the electrical length θ, one for $\tan\theta$ and the other for $-\tan\theta$. Once the terminal impedance Z_0 and the electrical length θ are determined, and the inequalities $Z_{1o}\tan^2\theta > Z_{2o}$ and $\tan^2\theta > 0$ are satisfied, the parameters such as Z_{1e}, Z_{2e}, R_1 and R_2 can be easily synthesized according to the analytical design equations (3) and (7). There is one degree of freedom in choosing the odd mode impedances Z_{1o}, Z_{2o}, and this can be used to control the relative coupling levels of the coupled line sections.

The smallest electrical length θ of the transmission line required for the dual-band operation is derived in [21].

$$\theta_1 = \frac{\pi}{1+t} \quad \theta_2 = \frac{t\pi}{1+t} \tag{16}$$

In the above, $t = f_2/f_1$ ($f_1 < f_2$), f_1 and f_2 designates the two band frequencies of the dual-band operation, θ_1 and θ_2 and corresponds to the electrical length θ of the transmission line at each band frequency, respectively. Either one of these can be substituted for θ in (3) and (7) to obtain the design data for the divider with a specified band ratio.

Previous studies [30]–[33] show that the power divider can realize dual frequency and wideband characteristics if the band ratio $t = f_2/f_1$ are determined reasonably. When the band ratio t is 2, the power divider shows broadband characteristic.

As mentioned previously, S_{11} and S_{12} depend on Z_{ie} ($i = 1, 2$) which is determined by the band ratio t, and S_{22}, S_{23} are dominated by Z_{io} ($i = 1, 2$). Fig. 3 and Fig. 4 show the relationship between $|S_{22}|$, $|S_{23}|$ and Z_{io} ($i = 1, 2$). Here, $c = Z_{io}/Z_{ie}$ ($c < 1$) ($i = 1, 2$). Therefore, we can calculate the odd impedances using (17).

$$Z_{io} = c \cdot Z_{ie} \quad (i = 1, 2) \tag{17}$$

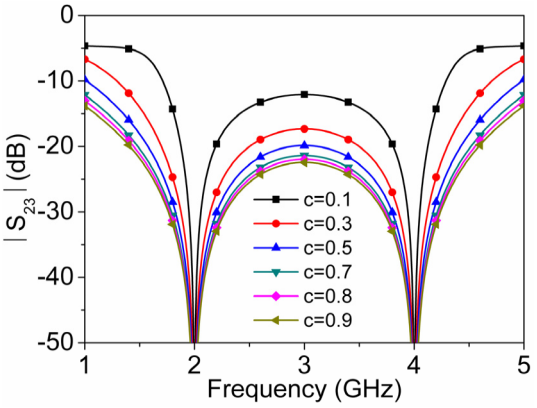

FIGURE 4. The relationship between Z_{io} (i=1.2) and $|S_{23}|$ with $f_2/f_1 = 2$.

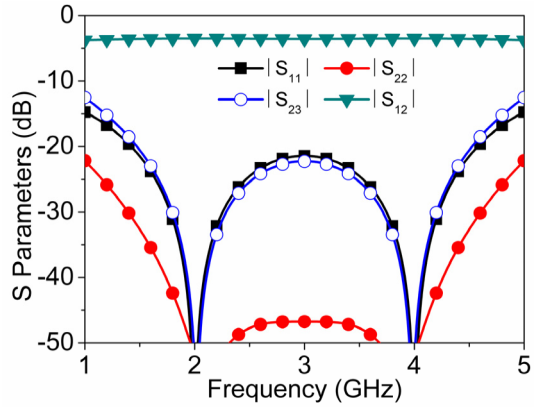

FIGURE 5. Calculated frequency responses of the divider.

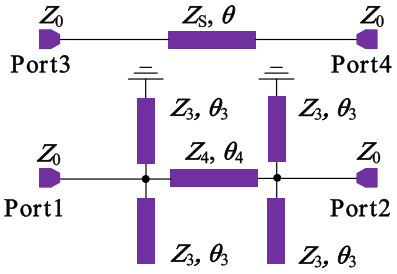

FIGURE 6. Equivalent circuit layout of the 90° phase shifter.

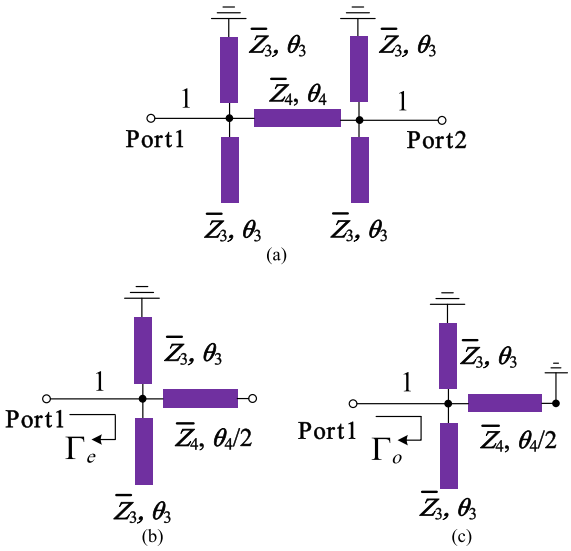

FIGURE 7. The normalized circuit (a) of the phase shifter and its equivalent circuit in even- (b) and odd-mode (c) excitations.

To design a wideband power divider, assuming that all ports are terminated in the characteristic impedance $Z_0 = 50\ \Omega$, we make $t = 2$, $c = 0.75$, and then $Z_{1e} = 79.3\ \Omega$, $Z_{2e} = 63.1\ \Omega$, $Z_{1o} = 59.5\ \Omega$, $Z_{2o} = 47.3\ \Omega$ are derived. We choose $R_1 = 82\ \Omega$ and $R_2 = 330\ \Omega$ which can correspond to commercial available values. The calculated frequency responses of the divider are shown in Fig. 5 with two bands of frequencies at 2 GHz and 4 GHz.

B. THEORETICAL ANALYSIS OF THE PHASE SHIFTER

The equivalent circuit of the 90° phase shifter is shown in Fig. 6, where Z_S stands for the characteristic impedance of the $3\lambda/4$ reference transmission line, Z_3 stands for the characteristic impedance of the shunted open- and short-circuited $\lambda/8$ transmission lines, Z_4 stands for the characteristic impedance of the $\lambda/2$ main transmission line.

Here $S_{33} = S_{44} = 0$, the scattering parameters of port 1 and port 2 can be obtained from the sum of the responses to the even and odd excitation.

Fig. 7 (a) illustrates the equivalent circuit of the shifter. For simplicity, all the impedance values of the 90° phase shifter are normalized to the port impedance. Fig. 7 (b) and (c) show the equivalent circuit in even- and odd- mode excitations. The scattering parameters of the phase shifter can be calculated from the reflection coefficients as

$$S_{11} = S_{22} = \frac{\Gamma_e + \Gamma_o}{2} \tag{18}$$

$$S_{12} = S_{21} = \frac{\Gamma_e - \Gamma_o}{2} \tag{19}$$

where Γ_e and Γ_o are reflection coefficients for the corresponding even- and odd-mode circuits, respectively, in turn can be calculated from the input port impedances or admittances as

$$\Gamma_i = \frac{Z_i - Z_0}{Z_i + Z_0} = \frac{\bar{Z}_i - 1}{\bar{Z}_i + 1} = \frac{1 - \bar{Y}_i}{1 + \bar{Y}_i} \quad i = e, o \tag{20}$$

with

$$\bar{Y}_e = j\bar{Y}_4 \tan\frac{\theta_4}{2} + j\bar{Y}_3 \tan\theta_3 - j\bar{Y}_3 \cot\theta_3 \tag{21}$$

$$\bar{Y}_o = -j\bar{Y}_4 \cot\frac{\theta_4}{2} + j\bar{Y}_3 \tan\theta_3 - j\bar{Y}_3 \cot\theta_3 \tag{22}$$

Now if we let $K_1 = \bar{Y}_4 \tan(\theta_4/2) - 2\bar{Y}_3 \cot 2\theta_3$ and $K_2 = \bar{Y}_4 \cot(\theta_4/2) + 2\bar{Y}_3 \cot 2\theta_3$, then we have

$$\bar{Y}_e = jK_1 \tag{23}$$

$$\bar{Y}_o = -jK_2 \tag{24}$$

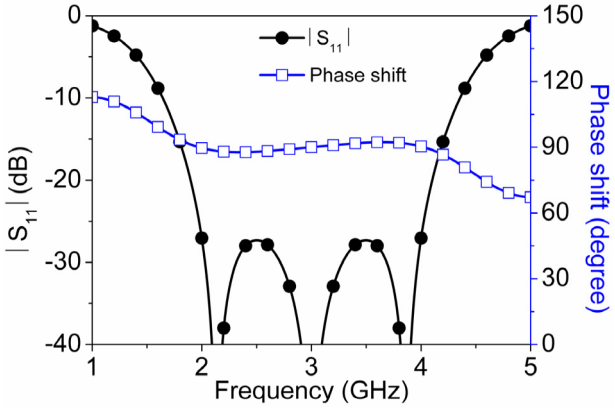

FIGURE 8. Calculated $|S_{11}|$ and phase shift of the phase shifter.

Using (21)-(24) in (20) yields

$$\Gamma_e = \frac{1 - jK_1}{1 + jK_1} \tag{25}$$

$$\Gamma_o = \frac{1 + jK_2}{1 - jK_2} \tag{26}$$

So we can obtain

$$S_{11} = S_{22} = \frac{1}{2}\left(\frac{1 - jK_1}{1 + jK_1} + \frac{1 + jK_2}{1 - jK_2}\right) \tag{27}$$

$$S_{12} = S_{21} = \frac{1}{2}\left(\frac{1 - jK_1}{1 + jK_1} - \frac{1 + jK_2}{1 - jK_2}\right) \tag{28}$$

The phase difference between the two branch line signals can be expressed as

$$\begin{aligned}\Delta\varphi &= \arg(S_{21}) - \arg(S_{43}) \\ &= \tan^{-1}\frac{1 + K_1(f)K_2(f)}{K_1(f) - K_2(f)} - \pi + \theta(f)\end{aligned} \tag{29}$$

where $\theta_3(f) = \bar{f}\pi/4$, $\theta_4(f) = \bar{f}\pi$, $\theta(f) = 3\pi\bar{f}/2$, $\bar{Y}_3$ and $\bar{Y}_4$ is normalized admittance, $\bar{f}$ is the normalized frequency, the central frequency is f_0.

$$\begin{cases} |\Gamma| = \dfrac{VSWR - 1}{VSWR + 1} \le 0.18 \\ |\Delta\varphi - \pi/2| \le 5\pi/180 \end{cases} \tag{30}$$

$$\bar{Y}_3 = 0.40, \quad \bar{Y}_4 = 0.81, \ 0.6 < \bar{f} < 1.4 \tag{31}$$

Assuming $VSWR \le 1.43$ ($S_{11} \le -15$dB) and the maximum phase difference is 5°, the unknowns $\bar{Y}_3$, $\bar{Y}_4$ and $\bar{f}$ can be obtained by solving equations of inequalities (30).

Then, we have $Z_3 = 2.5Z_0$, $Z_4 = 1.23Z_0$. Fig. 8 illustrates the calculated $|S_{11}|$ and phase shift of the phase shifter with the central frequency of 3 GHz.

III. IMPLEMENTATION AND RESULTS

A. CIRCUIT CONFIGURATION OF THE HYBRID COUPLER

The impedance parameters of the proposed hybrid coupler are expressed by the analysis of section II. Fig. 9 illustrates the design process.

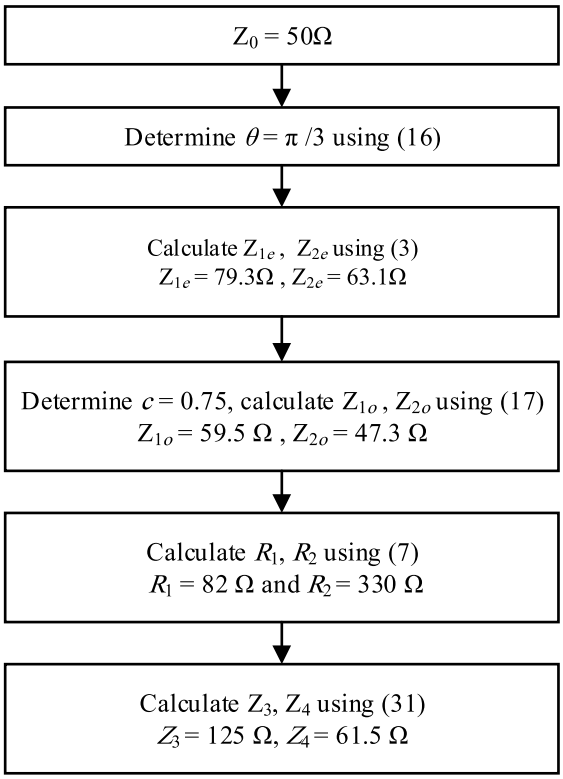

FIGURE 9. Design process of the coupler.

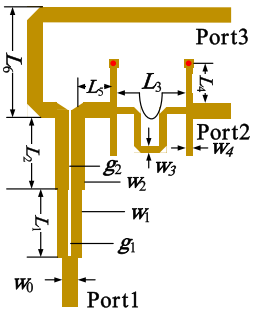

FIGURE 10. The layout of the proposed hybrid coupler. The critical dimensions are $w_0 = 2.7$ mm, $w_1 = 1.6$ mm, $w_2 = 2.4$ mm, $w_3 = 1.9$ mm, $w_4 = 0.37$ mm, $g_1 = 0.4$ mm, $g_2 = 0.6$ mm, $L_1 = 17.8$ mm, $L_2 = 17.4$ mm, $L_3 = 33.9$ mm, $L_4 = 8.9$ mm, $L_5 = 6.0$ mm, L 6 = 24.4 mm.

The hybrid coupler with the central frequency of 3 GHz was printed on the F4B-2 substrate with relative dielectric constant$\varepsilon_r = 2.65$, $\tan\delta = 0.001$ and thickness $h = 1.0$ mm. Fig. 10 illustrates the layout and all geometry parameters of the proposed hybrid coupler.

B. SIMULATIONS AND MEASUREMENTS

In this paper, the High Frequency Structure Simulator (HFSS) is utilized to accomplish the simulation and the optimization. The coupler is measured using Agilent E5071C series vector network analyzer. A photograph of the proposed hybrid coupler is shown in Fig. 11.

Port reflection coefficients of the hybrid coupler are illustrated in Fig. 12. The investigations show that the operating bandwidth defined by the reflection coefficient depends

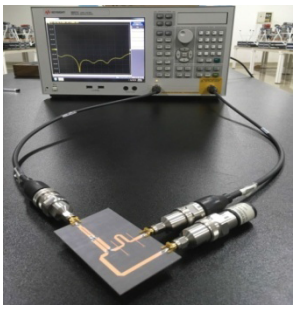

FIGURE 11. The photograph of the proposed hybrid coupler.

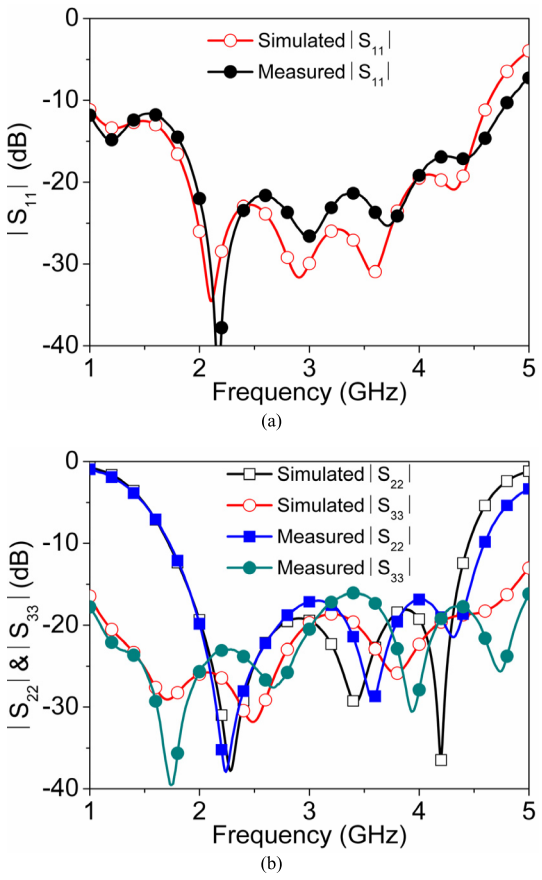

FIGURE 12. The port reflection coefficients of the proposed hybrid coupler. (a) $|S_{11}|$ and (b) $|S_{22}|$, $|S_{33}|$.

mainly on the parameter $|S_{22}|$, and the measured bandwidth for the reflection coefficients less than −15 dB is observed ranging from 1.89 GHz to 4.47 GHz.

Fig. 13. shows the power balance bandwidth of the hybrid coupler. The insertion loss ($|S_{12}|$, $|S_{13}|$) is less than 4 dB covering the frequency from 1.67 GHz to 4.42 GHz as the measured curves illustrated, in which the hybrid coupler delivers good impedance matching.

The isolation between the output ports of the hybrid coupler is shown in Fig. 14. The measured curves show that the worst port isolation ($|S_{23}|$) of is higher than 18 dB over the whole passband. Furthermore, ±5-degree phase difference between the two output ports is observed varying from 1.85 GHz to 4.42 GHz (85.7%).

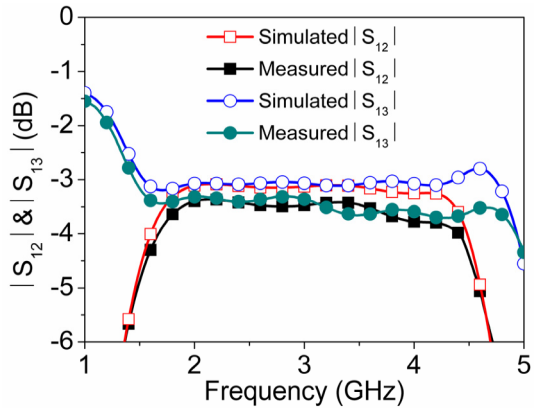

FIGURE 13. The power balance bandwidth of the proposed hybrid coupler.

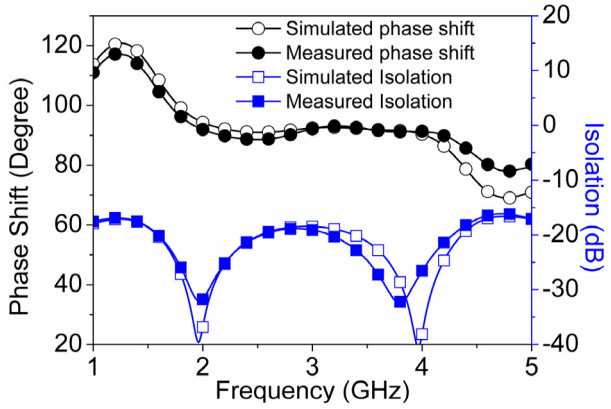

FIGURE 14. The phase shift and port isolation of the proposed hybrid coupler.

TABLE 1. Comparison with other reported works.

Ref.	f_0 (GHz)	$\|S_{11}\|$ 15-dB	Isolation (dB)	Multi-layer	Phase (±5°)
[4]	4.5	~42% (3.6-5.5GHz)	15	no	~44%
[12]	1.9	~76% (1.2-2.65GHz)	22	no	~55%
[13]	5.9	~57.6% (4.2-7.6GHz)	20	yes	~49%
[14]	6.8	~100% (3.1-10.6GHz)	18	yes	~100% (±10°)
[18]	2.4	~100% (0.45-2.8GHz)	20	no	~100%
[22]	3	75.7% (1.92-4.19GHz)	15 (1-5GHz)	no	43% (2.2-3.5GHz)
[27]	0.65	~62% (0.5-0.9GHz)	15 (0.4-0.84GHz)	no	84% (0.36-0.89GHz)
This work	3	92% (1.83-4.58GHz)	18 (1.46-4.42GHz)	no	85.7% (1.85-4.42GHz)

From what has been discussed above, the proposed coupler possesses a bandwidth of 84.3% (1.89-4.42 GHz) for the balance of impedance matching and phase shift. Table 1 summarizes the comparison of several 90° couplers in the literatures with our work. The presented coupler is much better

than [4], [12], [13], [22], [27] in terms of impedance matching and phase shift performance. Although [14] has ultra-wide bandwidth, multi-layer structure is usually incompatible with widely used single-layer components. Reference [18] used the Lange structure to achieve ultra-wide impedance matching and phase shift bandwidth, but its operating bandwidth is lower than 80% considering the power distribution performance.

IV. CONCLUSION

A wideband 90° hybrid coupler has been proposed in this paper. A pair of novel open- and short-circuit stub loaded structure is utilized to achieve the wideband 90-degree phase shifter, and two-section coupled-line Wilkinson power divider is combined to broaden the power dividing operating bandwidth of the hybrid coupler. The measured results demonstrate that the amplitude imbalance is less than 1 dB, the port isolation is better than 18 dB, and the phase variation is less than 5 degree over the whole passband. Good agreements between simulated and measured responses of the hybrid coupler are demonstrated, indicating that the proposed coupler has a promising application in multi-feed CP antennas and systems for wireless communication.

REFERENCES

[1] F. A. Ghaffar, M. K. Mobeen, S. Qamar, and M. Hasan, "A wide-band QPSK modulator using branch-line coupler and MESFET switches," in *Proc. MWSCAS*, Aug. 2009, pp. 1014–1017.

[2] Z. J. Jou, Y. Yang, L. Chiu, X. Zhu, E. Dutkiewicz, J. C. Vardaxoglou, and Q. Xue, "A W-band balanced power amplifier using broadside coupled strip-line coupler in SiGe BiCMOS 0.13-μ technology," *IEEE Trans. Circuits Syst. I, Reg. Papers*, vol. 65, no. 7, pp. 2139–2150, Dec. 2018.

[3] H.-J. Yoon and B.-W. Min, "Two section wideband 90° hybrid coupler using parallel-coupled three-line," *IEEE Microw. Wireless Compon. Lett.*, vol. 27, no. 6, pp. 548–550, Jun. 2017.

[4] J.-H. Cho, H.-Y. Hwang, and S.-W. Yun, "A design of wideband 3-dB coupler with N-section microstrip tandem structure," *IEEE Microw. Wireless Compon. Lett.*, vol. 15, no. 2, pp. 113–115, Feb. 2005.

[5] H. M. Liu, C. H. Xun, S. J. Fang, and D. Liu, "Coupled-line transdirectional coupler with arbitrary power divisions for equal complex termination impedances," *IET Microw., Antennas Propag.*, vol. 13, no. 1, pp. 92–98, 2019.

[6] R.-C. Han, S.-S. Zhong, and J. Liu, "Broadband circularly polarised dielectric resonator antenna fed by wideband switched line coupler," *Electron. Lett.*, vol. 50, no. 10, pp. 725–726, May 2014.

[7] Q. Liu, J. Shen, J. Yin, H. Liu, and Y. Liu, "Compact 0.92/2.45-GHz dual-band directional circularly polarized microstrip antenna for handheld RFID reader applications," *IEEE Trans. Antennas Propag.*, vol. 63, no. 9, pp. 3849–3856, Sep. 2015.

[8] Y. Shen, S.-G. Zhou, G.-L. Huang, and T.-H. Chio, "A compact dual circularly polarized microstrip patch array with interlaced sequentially rotated feed," *IEEE Trans. Antennas Propag.*, vol. 64, no. 11, pp. 4933–4936, Sep. 2016.

[9] D. M. Pozar, *Microwave Engineering*, 4th ed. Hoboken, NJ, USA: Wiley, 2012.

[10] C.-W. Tang, M.-G. Chen, Y.-S. Lin, and J.-W. Wu, "Broadband microstrip branch-line coupler with defected ground structure," *Electron. Lett.*, vol. 42, no. 25, pp. 1458–1460, Dec. 2006.

[11] Y.-H. Chun and J.-S. Hong, "Compact wide-band branch-line hybrids," *IEEE Trans. Microw. Theory Techn.*, vol. 54, no. 2, pp. 704–709, Feb. 2006.

[12] H.-J. Yoon and B.-W. Min, "Two section wideband 90° hybrid coupler using parallel-coupled three-line," *IEEE Microw. Wireless Compon. Lett.*, vol. 27, no. 6, pp. 548–550, Jun. 2017.

[13] W. A. Arriola, J. Y. Lee, and I. S. Kim, "Wideband 3 dB branch line coupler based on λ/4 open circuited coupled lines," *IEEE Microw. Wireless Compon. Lett.*, vol. 21, no. 9, pp. 486–488, Sep. 2011.

[14] D. N. A. Zaidel, S. K. A. Rahim, N. Seman, C. L. Chew, and N. H. Khamis, "A design of octagon-shaped 3-dB ultra wideband coupler using multilayer technology," *Microw. Opt. Technol. Lett.*, vol. 55, no. 1, pp. 127–130, Jan. 2013.

[15] M. Nedil, T. A. Denidni, and L. Talbi, "Design of a new directional coupler using CPW multilayer technology," *Microw. Opt. Technol. Lett.*, vol. 48, no. 3, pp. 471–474, Mar. 2006.

[16] J. Lange, "Interdigitated stripline quadrature hybrid," *IEEE Trans. Microw. Theory Techn.*, vol. MTT-17, no. 12, pp. 1150–1151, Dec. 1969.

[17] R. M. Osmani, "Synthesis of lange couplers," *IEEE Trans. Microw. Theory Techn.*, vol. MTT-29, no. 2, pp. 168–170, Feb. 1981.

[18] J.-C. Chiu, C.-M. Lin, and Y.-H. Wang, "A 3-dB quadrature coupler suitable for PCB circuit design," *IEEE Trans. Microw. Theory Techn.*, vol. 54, no. 9, pp. 3521–3525, Sep. 2006.

[19] K. Janisz, R. Smolarz, A. Rydosz, K. Wincza, and S. Gruszczynski, "Compensated 3-dB lange directional coupler in suspended microstrip technique," in *Proc. MAPE*, Oct. 2017, pp. 1–4.

[20] Z.-Y. Zhang, Y.-X. Guo, L. C. Ong, and M. Y. W. Chia, "A new wide-band planar balun on a single-layer PCB," *IEEE Microw. Wireless Compon. Lett.*, vol. 15, no. 6, pp. 416–418, Jun. 2005.

[21] S. Y. Eom, "Broadband 180° bit phase shifter using a λ/2 coupled line and parallel λ/8 stubs," *IEEE Microw. Wireless Compon. Lett.*, vol. 14, no. 5, pp. 228–230, May 2004.

[22] Y. Wu, Q. Liu, J. Shen, and Y. Liu, "A novel wide-band hybrid coupler using coupled-line power divider and improved coupled-line phase shifter," *J. Electromagn. Waves Appl.*, vol. 27, no. 3, pp. 374–384, Nov. 2013.

[23] B. M. Schiffman, "A new class of broad-band microwave 90-degree phase shifters," *IRE Trans. Microw. Theory Techn.*, vol. 6, no. 2, pp. 232–237, Apr. 1958.

[24] J. L. R. Quirarte and J. P. Starski, "Novel Schiffman phase shifters," *IEEE Trans. Microw. Theory Techn.*, vol. 41, no. 1, pp. 9–14, Jan. 1993.

[25] Y.-X. Guo, Z.-Y. Zhang, and L. Ong, "Improved wide-band Schiffman phase shifter," *IEEE Trans. Microw. Theory Techn.*, vol. 54, no. 3, pp. 1196–1200, Mar. 2006.

[26] Y. X. Xin, B.-Z. Wang, J. He, and Q. Q. He, "A novel Schiffman phase shifter with a defected microstrip structure," *J. Electromagn. Waves Appl.*, vol. 22, pp. 187–193, Jan. 2008.

[27] E. Jafari, F. Hodjatkashani, and R. Rezaiesarlak, "A broadband quadrature hybrid using improved wideband Schiffman phase shifter," *Prog. Electromagn. Res. C*, vol. 11, pp. 229–236, 2009.

[28] L. Guo and A. Abbosh, "Phase shifters with wide range of phase and ultra-wideband performance using stub-loaded coupled structure," *IEEE Microw. Wireless Compon. Lett.*, vol. 24, no. 3, pp. 167–169, Mar. 2014.

[29] H.-R. Ahn, *Asymmetric Passive Components in Microwave Integrated Circuits*. Hoboken, NJ, USA: Wiley, 2006, pp. 29–41.

[30] M. J. Park, "Dual-band Wilkinson divider with coupled output port extensions," *IEEE Trans. Microw. Theory Techn.*, vol. 57, no. 9, pp. 2232–2237, Sep. 2009.

[31] Y. Wu, Y. Liu, and Q. Xue, "An analytical approach for a novel coupled-line dual-band Wilkinson power divider," *IEEE Trans. Microw. Theory Techn.*, vol. 59, no. 2, pp. 286–294, Feb. 2011.

[32] M.-J. Park, B. Lee, and M.-J. Park, "Dual-band Wilkinson power divider-with shifted output ports," *IEEE Microw. Wireless Compon. Lett.*, vol. 18, no. 7, pp. 443–445, Jul. 2008.

[33] X. Tang and K. Mouthaan, "Analysis and design of compact two-way Wilkinson power dividers using coupled lines," in *Proc. Asia–Pacific Microw. Conf.*, Dec. 2009, pp. 1319–1322.

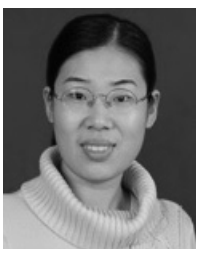

RUYING SUN received the B.S. degree in electronic engineering from Ludong University, Yantai, China, in 2003, and the M.S. degree from Chongqing University, Chongqing, China, in 2006. She is currently pursuing the Ph.D. degree in information and communication engineering with Wuhan University, Wuhan, China. Since 2006, she has been with the Department of Electronic Engineering, Linyi University, China. Her research interests include microwave and millimeter wave circuits, antennas, and wireless communications.

QINGHU CHEN received the Ph.D. degree from the Huazhong University of Science and Technology, in 1998. He is currently a Professor with Wuhan University. His research interests include wireless communication, pattern recognition, and intelligent systems.

RONGCANG HAN received the B.S. degree from Ludong University, Yantai, China, in 2003, the M.S. degree from the University of Electronic Science and Technology of China, Chengdu, China, in 2006, and the Ph.D. degree from Shanghai University, Shanghai, China, in 2016, all in electronic engineering. Since 2006, he has been with the Department of Physics, Linyi University, China, where he is currently an Assistant Professor with the Department of Electronic Engineering. His research interests include dielectric resonator antennas, microstrip antennas, and microwave circuits.

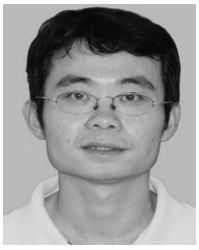

ZHONGLIANG LU received the B.S. degree in electronic engineering from Nanchang University, Nanchang, China, in 2003, the M.S. degree from the South China University of Science and Technology, Guangzhou, China, in 2006, and the Ph.D. degree from Shanghai University, Shanghai, China, in 2016, all in electronic engineering. Since 2006, he has been with the School of Information Engineering, Jiangxi University of Science and Technology, Ganzhou, China, where he is currently an Assistant Professor. His research interests include reconfigurable antennas, conformal antennas, and microwave circuits.